

Nuclear Science and Engineering



ISSN: 0029-5639 (Print) 1943-748X (Online) Journal homepage: https://www.tandfonline.com/loi/unse20

Ray Effect Mitigation for the Discrete Ordinates Method Using Artificial Scattering

Martin Frank, Jonas Kusch, Thomas Camminady & Cory D. Hauck

To cite this article: Martin Frank, Jonas Kusch, Thomas Camminady & Cory D. Hauck (2020): Ray Effect Mitigation for the Discrete Ordinates Method Using Artificial Scattering, Nuclear Science and Engineering, DOI: <u>10.1080/00295639.2020.1730665</u>

To link to this article: https://doi.org/10.1080/00295639.2020.1730665

Published online: 17 Mar 2020.	
Submit your article to this journal 🗹	
Article views: 46	
View related articles 🗷	
View Crossmark data ☑	





Ray Effect Mitigation for the Discrete Ordinates Method Using Artificial Scattering

Martin Frank, ** Jonas Kusch, * Thomas Camminady, * and Cory D. Hauck *b,c

Received November 19, 2019 Accepted for Publication February 13, 2020

Abstract — Solving the radiative transfer equation with the discrete ordinates (S_N) method leads to a nonphysical imprint of the chosen quadrature set on the solution. To mitigate these so-called ray effects, we propose a modification of the S_N method that we call artificial scattering S_N (as- S_N). The method adds an artificial forward-peaked scattering operator that generates angular diffusion to the solution and thereby mitigates ray effects. Similar to artificial viscosity for spatial discretizations, the additional term vanishes as the number of ordinates approaches infinity. Our method allows an efficient implementation of explicit and implicit time integration according to standard S_N solver technology. For two test cases, we demonstrate a significant reduction of error for the as- S_N method when compared to the standard S_N method, both for explicit and implicit computations. Furthermore, we show that a prescribed numerical precision can be reached with less memory due to the reduction in the number of ordinates.

Keywords — Discrete ordinates method, ray effects, radiative transfer, quadrature.

Note — Some figures may be in color only in the electronic version.

I. INTRODUCTION

Several applications in the field of physics require an accurate solution of the radiative transfer equation. This equation describes the evolution of the angular flux of particles moving through a material medium. Examples include nuclear engineering, 1,2 high-energy astrophysics, 3,4 supernovae, 5,6 and fusion. 7,8 A major challenge when solving the radiative transfer equation numerically is the high-dimensional phase-space on which it is defined. There are three spatial dimensions, two directional (angular) parameters, velocity, and time. In many applications, there is additional frequency or energy dependence. Hence, numerical methods to approximate the solution require a carefully chosen phase-space discretization.

There are several strategies to discretize the angular variables, and they all have certain strengths and

weaknesses. The spherical harmonics (P_N) method $^{10-12}$ is a spectral Galerkin discretization of the radiative transfer equation. It uses the spherical harmonics basis functions to represent the solution in terms of angular variables with finitely many expansion coefficients, called moments. The P_N method preserves rotational symmetry and shows spectral convergence for smooth solutions.

However, like most spectral methods, P_N yields oscillatory solution approximations in nonsmooth regimes, which can lead to negative, nonphysical angular flux values.¹³ Filtering of the expansion coefficients has been shown to mitigate oscillations,¹⁴ and a modified equation analysis has shown that filtering adds an artificial forward-peaked scattering operator to the equation if a certain scaling strength of the filter is chosen.

The discrete ordinates (S_N) method¹² approximates the radiative transfer equation on a set of discrete angular directions. The S_N discretization preserves positivity of the angular flux while yielding an efficient and straightforward

^aKarlsruhe Institute of Technology, Karlsruhe, Germany

^bOak Ridge National Laboratory, Oak Ridge, Tennessee

^cUniversity of Tennessee, Knoxville Tennessee

^{*}E-mail: martin.frank@kit.edu

implementation of time-implicit methods. However, the method is plagued by numerical artifacts, know as ray effects, when there are not enough ordinates to resolve the angular flux. Because increasing the number of ordinates significantly increases numerical costs of simulations, a major task to improve the solution accuracy of S_N methods is to mitigate these ray effects 15–17 without simply adding more ordinates.

Various strategies to mitigate ray effects at affordable costs have been developed. Reference 18 uses a biased quadrature set, which reflects the importance of certain ordinates. Furthermore, Ref. 19 presents a method combining the P_N method with the S_N method. Further studies for this method can be found in Refs. 20, 21, and 22, which show a reduction of ray effects. In Ref. 16, a comparison of these methods can be found. In Ref. 23, computing the angular flux for differently oriented quadrature sets and averaging over different solutions have been proposed to reduce ray artifacts. In Ref. 24, a rotated S_N method has been developed that rotates the quadrature set after every time iteration. Consequently, particles can move on a heavily increased set of directions of travel, leading to a reduction of ray effects. Analytic results show that rotating the quadrature set plays the role of an angular diffusion operator, which smears out artifacts that stem from the finite number of ordinates. Unfortunately, this method does not allow a straightforward implementation of sweeping, complicating the use of implicit methods.

The idea of this work is to add angular diffusion directly with the help of a forward-peaked artificial scattering operator. We choose this operator so that the effect of artificial scattering vanishes in the limit of infinitely many ordinates but at finite order adds angular diffusion in such a way that it mitigates ray effects. Unlike the rotated S_N method in Ref. 24, the current approach allows for a straightforward implementation of sweeping, which we use to implement an implicit method.

II. MAIN IDEA

In this section, we summarize the relevant mathematical background and introduce notation. We illustrate the problem of ray effects that occurs when discretizing the transport equation in angle and how artificial scattering can be used to mitigate these ray effects. We demonstrate that artificial scattering behaves like a Fokker-Planck operator in the appropriate limit.

II.A. Radiative Transfer Equation

The radiative transfer equation describes the evolution of the angular flux $\psi(t, \mathbf{x}, \Omega)$ via

$$\hat{\sigma}_t \psi(t, \mathbf{x}, \Omega) + \Omega \cdot \nabla_{\mathbf{x}} \psi(t, \mathbf{x}, \Omega) + \sigma_t(\mathbf{x}) \psi(t, \mathbf{x}, \Omega)
= \sigma_s(\mathbf{x}) (S^+ \psi)(t, \mathbf{x}, \Omega) + q(t, \mathbf{x}),$$
(1)

where $t \in \mathbb{R}_+ = \text{time},$ $x \in \mathbb{R}^3 = \text{spatial variable},$ $\Omega \in \mathbb{S}^2 = \text{direction}.$

The total cross section is $\sigma_t(\mathbf{x}) = \sigma_a(\mathbf{x}) + \sigma_s(\mathbf{x})$. In the case of scattering, the in-scattering kernel operator $S^+(\psi)(t,\mathbf{x},\Omega)$ describes the gain of particles that were previously traveling along direction Ω' and changed to direction Ω . It is given by

$$(S^{+}\psi)(t, \mathbf{x}, \Omega) = \int_{\mathbb{S}^{2}} s(\Omega \cdot \Omega') \psi(t, \mathbf{x}, \Omega') d\Omega', \qquad (2)$$

where $s(\Omega \cdot \Omega')$ is the probability of transitioning from direction Ω' into direction Ω or vice versa. For simplicity, we assume that the source q(t, x) is isotropic.

II.B. Ray Effects

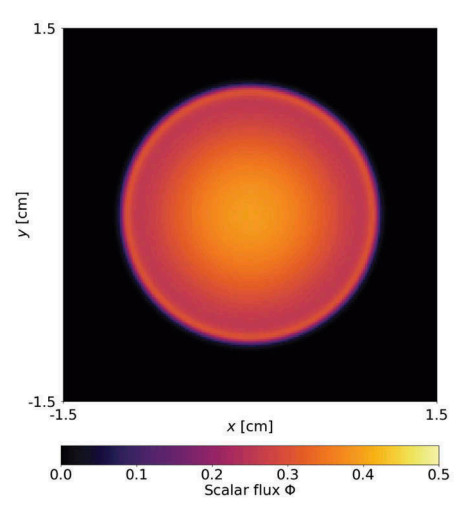
As previously explained, the S_N method preserves positivity but suffers from ray effects. An example of these artifacts is demonstrated for the line-source benchmark in Fig. 1. While the true scalar flux $\Phi(t, \mathbf{x}) := \int_{\mathbb{S}^2} \psi(t, \mathbf{x}, \Omega') d\Omega'$ is radially symmetric, the numerical solution has artifacts in the form of oscillations. We will discuss the line-source problem in more detail in Sec. IV.A.

II.C. Artificial Scattering

We propose to address the problem of ray effects by adding artificial scattering to the right-hand side (RHS) of Eq. (1), in the form of an anisotropic scattering operator. The modified system is then

$$\partial_t \psi(t, \mathbf{x}, \Omega) + \Omega \cdot \nabla_{\mathbf{x}} \psi(t, \mathbf{x}, \Omega) + \sigma_t(\mathbf{x}) \psi(t, \mathbf{x}, \Omega)
= \sigma_s(\mathbf{x}) (S^+ \psi)(t, \mathbf{x}, \Omega)
+ \sigma_{as}(\mathbf{x}) (S_{as} \psi)(t, \mathbf{x}, \Omega) + q(t, \mathbf{x}),$$
(3)

where



(a) The semi-analytical reference solution to the line source problem.

Fig. 1. Illustrating ray effects with the line-source problem.

(b) Numerical solution using the S_N method with a product quadrature. Ray effects are clearly visible.

$$\sigma_{as}(\mathbf{x})(S_{as}\psi)(t,\mathbf{x},\Omega) = \sigma_{as}(\mathbf{x}) \int_{\mathbb{S}^2} s_{\varepsilon}(\Omega' \cdot \Omega)(\psi(t,\mathbf{x},\Omega') - \psi(t,\mathbf{x},\Omega)) d\Omega',$$
(4)

where s_{ε} can be any Dirac-like sequence, a i.e.,

$$\int_{-1}^{+1} s_{\varepsilon}(\mu) d\mu = 1$$
and
$$\int_{-1}^{+1} s_{\varepsilon}(\mu) f(\mu) d\mu \to f(1)$$
(5)

for any sufficiently smooth function f as $\epsilon \to 0$. In our experiments, we choose

$$s_{\varepsilon}(\mu) = \frac{2}{\sqrt{\pi} \varepsilon \operatorname{Erf}\left(\frac{2}{\varepsilon}\right)} e^{-(1-\mu)^{2}/\varepsilon^{2}}, \qquad (6)$$

where the error function satisfies $\operatorname{Erf}(x) \to 1$ as $x \to \infty$. The proposed method, which we call artificial scattering- S_N (as- S_N), has the following effects:

1. Similar to the artificial viscosity used to stabilize spatial discretizations of hyperbolic operators (Ref. 25, Chap. 16.1), the artificial scattering adds an angular diffusion term to the radiative transfer equations. This term should vanish when the discretization is refined. Therefore,

the variance of the artificial scattering kernel should be chosen to vanish in the limit $N_q \to \infty$. We choose the variance to be $\varepsilon = \beta/N_q$, where β is a constant, user-determined parameter. This choice ensures that ε scales the average width of quadrature points, meaning that the domain of influence includes roughly the same number of ordinates when N_q increases. In the limit, the as- S_N solution converges to the classical S_N solution.

- 2. The total number of particles is preserved by the artificial scattering term. Higher-order moments are however dampened by the magnitude of artificial scattering. A beam of particles inside a void will be subject to scattering by the as- S_N method; however, artifacts that result from the standard S_N method dominate the overall error, unless the beam is aligned with the quadrature set.
- 3. Artificial scattering has been used for the P_N method to mitigate oscillations.²⁶ Besides using artificial scattering on the ordinates level, we are using a forward-peaked scattering kernel instead of isotropic scattering. Hence, the as- S_N modification scatters around the direction of the original ordinates.
- 4. The as- S_N method has similarities to the P_{N-1} -equivalent S_N method.²² To mitigate ray effects, this method adds a fictitious source to the radiative transfer equation. This source, though derived by a different strategy, requires similar modifications of the standard S_N implementation. The main difference is that the artificial scattering kernel of as- S_N is forward peaked, which can be used to design an efficient numerical treatment. Note that the P_{N-1} -equivalent S_N method will have the same problems as P_N .



^a While the idea of artificial scattering works with any Dirac sequence, the asymptotic analysis that is performed later imposes stronger requirements to obtain a Fokker-Planck operator in the respective limit.

- 5. Since the artificial scattering acts as a filter on the moment level, as- S_N can be compared to filtered P_N (Refs. 14 and 27). Note that a convergence proof for filtered P_N can be found in Ref. 28, which can be used to study effects of artificial scattering, similar to Ref. 27.
- 6. With appropriate boundary and initial conditions, the as- S_N Eq. (3) can be solved in a straightforward manner using common S_N implementations. When discussing one such implementation, we will focus on implicit discretization techniques and derive an efficient algorithm to treat the artificial scattering term.

II.D. Artificial Scattering Kernel

To better distinguish between the two types of scattering, we will call the naturally occurring scattering of Eq. (1) "physical scattering" and the scattering in Eq. (4) "artificial scattering." The way the artificial scattering is written in Eq. (4), it includes in-scattering and outscattering. We can split this further into

$$(S_{as}\psi)(t, \mathbf{x}, \Omega) = \int_{\mathbb{S}^2} s_{\varepsilon}(\Omega' \cdot \Omega)$$
$$(\psi(t, \mathbf{x}, \Omega') - \psi(t, \mathbf{x}, \Omega)) d\Omega'$$
$$= (S_{as}^+\psi)(t, \mathbf{x}, \Omega) - (S_{as}^-\psi)(t, \mathbf{x}, \Omega)$$
(7)

with

$$(S_{as}^{+}\psi)(t, \mathbf{x}, \Omega) = \int_{\mathbb{S}^{2}} s_{\varepsilon}(\Omega' \cdot \Omega)\psi(t, \mathbf{x}, \Omega') d\Omega'$$
 (8)

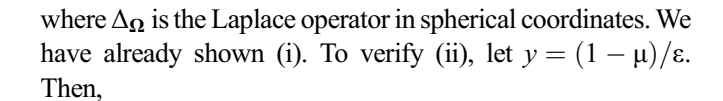
and

$$(S_{as}^{-}\psi)(t, \mathbf{x}, \Omega) = \psi(t, \mathbf{x}, \Omega). \tag{9}$$

II.E. Modified Equation Analysis

According to Pomraning,²⁹ the Fokker-Planck operator can be a legitimate description of highly peaked scattering. This is true if (i) the scattering kernel $s_{\epsilon}(\mu)$ is a Dirac sequence and (ii) the transport coefficients $p_{\epsilon,i} := \int_{-1}^{+1} (1-\mu)^i s_{\epsilon}(\mu) \, d\mu$ are of order $\mathcal{O}(\epsilon^i)$. The resulting modified equation then reads

$$\partial_t \psi(t, \mathbf{x}, \Omega) + \Omega \cdot \nabla_{\mathbf{x}} \psi + (\sigma_a + \sigma_s) \psi
= \sigma_s \cdot \Phi + \pi \cdot p_{\varepsilon, 1} \cdot \sigma_{as} \cdot \Delta_{\Omega} \psi + O(\varepsilon^2), \quad (10)$$



$$p_{\varepsilon,i} = \int_{2/\varepsilon}^{0} (\varepsilon y)^{i} \frac{2}{\sqrt{\pi} \varepsilon \operatorname{Erf}\left(\frac{2}{\varepsilon}\right)} e^{-y^{2}} (-\varepsilon) \, dy \tag{11}$$

$$= \frac{2}{\sqrt{\pi}\varepsilon \operatorname{Erf}\left(\frac{2}{F}\right)} \varepsilon^{i} \int_{0}^{2/\varepsilon} y^{i} e^{-y^{2}} dy \tag{12}$$

$$= \frac{2}{\sqrt{\pi} \varepsilon \operatorname{Erf}\left(\frac{2}{\varepsilon}\right)} \varepsilon^{i} \left[\Gamma\left(\frac{1+i}{2}\right) - \Gamma\left(\frac{1+i}{2}, \frac{4}{\varepsilon^{2}}\right) \right]$$
(13)

$$= \mathcal{O}(\varepsilon^i) \,, \tag{14}$$

where $\Gamma(\cdot)$ and $\Gamma(\cdot,\cdot)$ denote the gamma function and the upper incomplete gamma function, respectively. Since (ii) implies that $p_{\epsilon,1}=\mathcal{O}(\epsilon)$, the operator vanishes if we let $\epsilon\to 0$.

We set $\varepsilon = \beta/N_q$ in the discrete case so that the angular diffusion vanishes if the number of ordinates N_q tends to infinity. This analysis shows that the product $\sigma_{as} \cdot \beta$ controls the strength of the added angular diffusion. Section IV.A confirms this numerically.

III. DISCRETIZATION

In this section, we discuss discretization and implementation of the presented as- S_N method, laying the focus on how to incorporate artificial scattering into existing S_N codes.

III.A. S_N Discretization

For the sake of completeness, we briefly summarize the S_N method. Given a finite number of ordinates $\Omega_1, \ldots, \Omega_{N_q}$ and defining the S_N solution $\psi_q(t, \mathbf{x}) \approx \psi(t, \mathbf{x}, \Omega_q)$, the S_N method solves the semidiscretized system of N_q equations:

$$\partial_t \psi_q(t, \mathbf{x}) + \Omega_q \cdot \nabla_{\mathbf{x}} \psi_q(t, \mathbf{x}) + \sigma_t(\mathbf{x}) \psi_q(t, \mathbf{x})
= \sigma_s(\mathbf{x}) \sum_{p=1}^{N_q} w_p \cdot s(\Omega_q \cdot \Omega_p) \psi_p(t, \mathbf{x}) + q(t, \mathbf{x}) . (15)$$

Here, w_p are quadrature weights, chosen such that

$$\int_{\mathbb{S}^2} \Psi(t, \boldsymbol{x}, \Omega) d\Omega \approx \sum_{q=1}^{N_q} w_q \cdot \Psi(t, \boldsymbol{x}, \Omega_q).$$
 (16)

To compute numerical solutions, we still need to discretize Eq. (15) in space and time. In this work, we will investigate solutions for both implicit and explicit time discretizations. The explicit code uses Heun's method as well as a minmod slope limiter. It is based on Refs. 24 and 30, which provide a detailed description of the chosen methods. The implicit discretization and an efficient strategy to integrate artificial scattering in a given implicit code framework will be discussed in Secs. III.D and III.E.

III.B. Adding Artificial Scattering to the S_N equations

Our goal is to include artificial scattering in the S_N equations in Eq. (15). By simply approximating the artificial scattering term in Eq. (3) with the chosen quadrature rule, we obtain the as- S_N equation:

$$\begin{aligned}
\partial_{t}\psi_{q}(t, \mathbf{x}) + \Omega_{q} \cdot \nabla_{\mathbf{x}}\psi_{q}(t, \mathbf{x}) + \sigma_{t}(\mathbf{x})\psi_{q}(t, \mathbf{x}) \\
+ \sigma_{as}(\mathbf{x})\psi_{q}(t, \mathbf{x}) \\
&= \sigma_{s}(\mathbf{x}) \sum_{p=1}^{N_{q}} w_{p} \cdot c_{q} \cdot s(\Omega_{q} \cdot \Omega_{p})\psi_{p}(t, \mathbf{x}) \\
+ \sigma_{as}(\mathbf{x}) \sum_{p=1}^{N_{q}} w_{p} \cdot c_{q}^{(\varepsilon)} \cdot s_{\varepsilon}(\Omega_{q} \cdot \Omega_{p})\psi_{p}(t, \mathbf{x}) \\
+ q(t, \mathbf{x}), & (17)
\end{aligned}$$

where $c_q=1/\sum_p w_p \cdot s(\Omega_q \cdot \Omega_p)$ and $c_q^{(\epsilon)}=1/\sum_p w_p \cdot s_\epsilon(\Omega_q \cdot \Omega_p)$ are normalization factors. While on the continuous level, these factors are the same for every direction, we obtain a dependency on the chosen ordinate due to the nonuniform discretization in angle. These normalization factors are needed to obtain a simple expression for the outscattering terms. Moving these terms to the left-hand side (LHS) of Eq. (17) stabilizes the source iteration used in the implicit method.

III.C. Quadrature

It remains to pick an adequate quadrature set. When applying artificial scattering, the solution smears out along the directions in the quadrature set. To ensure an evenly spread artificial scattering effect, a quadrature with a highly uniform ordinate distribution should be chosen. Commonly, the construction of a quadrature set starts at a chosen planar geometry, which is discretized and then mapped onto the surface of a sphere. The mapped nodes of the previously chosen discretization are then taken to be the quadrature points while the weights are determined by the area associated with

these points. An even node distribution is achieved by using an icosahedron as the initial planar geometry, which one can find in Fig. 2. Each face of the icosahedron is triangulated to generate the nodes that will be mapped onto the surface of the sphere. There are different strategies to perform this triangulation, and we choose an equidistant spacing of points on each line of the triangle as well as the corresponding points inside the triangle. The corresponding weight is the area of the hexagon that lies around the given node and is defined by connecting the midpoints of the neighboring triangles. For more details on the icosahedron quadrature, see Ref. 31. From now on, we will exclusively use this quadrature in all S_N and as- S_N computations. A sample of the icosahedron quadrature can be found in Appendix A.

III.D. Implicit Time Discretization

Implicit time discretization methods provide stability for large time steps, which are crucial in applications involving different timescales. However, when discretizing the radiative transfer equation, they require a matrix solve in every time step, which is commonly performed by a Krylov solver.^{32,33} We start with an implicit Euler discretization, where in an abuse of notation, we denote

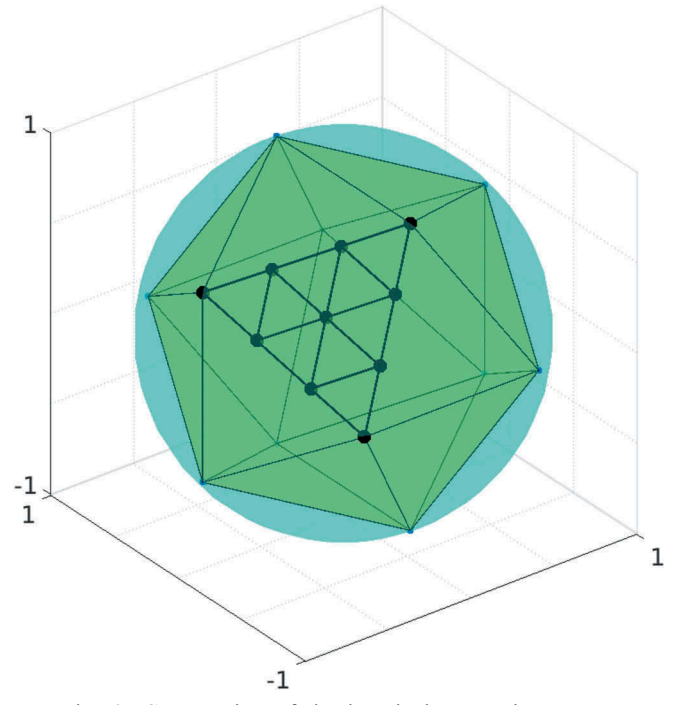


Fig. 2. Construction of the icosahedron quadrature set. One can see the icosahedron geometry with a triangulated face that is then mapped onto the sphere. For the quadrature set, we align one of the vertices with the point (0,0,1).



the flux at the new time step by $\psi(x, \Omega)$ and at the old time step by $\psi^{old}(x, \Omega)$. The equivalent as-S_N system is

$$\mathbf{\Omega} \cdot \nabla_{\mathbf{x}} \Psi + \left(\sigma_{a} + \sigma_{s} + \sigma_{as} + \frac{1}{\Delta t} \right) \Psi
= \sigma_{s} S^{+} \Psi + \sigma_{as} S^{+}_{as} \Psi + q + \frac{\Psi^{old}}{\Delta t} .$$
(18)

Defining the streaming operator $L\psi = \Omega \cdot \nabla_x \psi + (\sigma_a + \sigma_s + \sigma_{as} + \frac{1}{\Delta t})\psi$ as well as the modified source $\tilde{q} = q + \psi^{old}/\Delta t$, we can put this into more compact notation:

$$L\psi = \sigma_s S^+ \psi + \sigma_{as} S^+_{as} \psi + \widetilde{q} . \tag{19}$$

First, let us numerically treat the artificial scattering in the same way as commonly done for physical scattering. The physical in-scattering kernel can be written as

$$S^+ = O\Sigma M$$
,

where Σ carries the respective expansion coefficients of the scattering kernel and M maps from the ordinates to the moments and O from the moments back to the angular space. Making use of this strategy to represent the artificial scattering, we get

$$S_{as}^{+} = O\Sigma_{as}M. (20)$$

When denoting the moments as $\phi = M\psi$, Eq. (19) becomes

$$L\Psi = \sigma_s O \Sigma \phi + \sigma_{as} O \Sigma_{as} \phi + \widetilde{q} . \tag{21}$$

Inverting L and applying M to both sides yield the fixed-point equation:

$$\phi = \sigma_s M L^{-1} O \Sigma \phi + \sigma_{as} M L^{-1} O \Sigma_{as} \phi + M L^{-1} \widetilde{q} . \qquad (22)$$

Note that with $\sigma_{as} = 0$, this is the standard equation to which a Krylov solver is applied. Choosing a nonzero artificial

scattering strength can result in significantly increased numerical costs when solving Eq. (22) with a Krylov method: To show this, let us move to the discrete level, i.e., discretizing the directional domain, which requires picking a finite number of moments. In this case Σ becomes a diagonal matrix with entries falling rapidly to zero (in the case of isotropic scattering, only the first entry is nonzero). Hence, few moments are required to capture the effects of physical scattering. However, since the artificial scattering kernel is strongly forward peaked, the entries of the diagonal matrix Σ_{as} do not fall to zero quickly, meaning that the method requires a large number of moments to include artificial scattering, which results in a heavily increased run time.²⁷ The slow decay of the Legendre moments

$$k_{\varepsilon,n} = 2\pi \int_{-1}^{+1} s_{\varepsilon}(\mu) P_n(\mu) d\mu$$
 for $\varepsilon \to 0$ is visualized in Fig. 3.

In order to be able to choose the reduced number of moments required to resolve physical scattering, we move the artificial scattering into the sweeping step. Hence, going back to Eq. (19), we only perform the moment decomposition on the physical scattering to obtain

$$(L - \sigma_{as} S_{as}^{+}) \psi = \sigma_{s} O \Sigma \phi + \widetilde{q} . \tag{23}$$

Moving the operator $(L - \sigma_{as}S_{as}^+)$ to the RHS and taking moments yield

$$\phi = \sigma_s M (L - \sigma_{as} S_{as}^+)^{-1} O \Sigma \phi + M (L - \sigma_{as} S_{as}^+)^{-1} \widetilde{q} . \tag{24}$$

The Krylov solver is then applied to this fixed-point iteration. In contrast to Eq. (22), the physical scattering term dictates the number of moments. The computation of $(L - \sigma_{as}S_{as}^+)^{-1}$ is performed by a source iteration, where the general equation $(L - \sigma_{as}S_{as}^+)\psi = R$ is solved by iterating on

$$L\psi^{(l+1)} = \sigma_{as}S^{+}_{as}\psi^{(l)} + R.$$
 (25)

This iteration is expected to converge fast since effects of artificial scattering will be small in comparison to physical scattering.

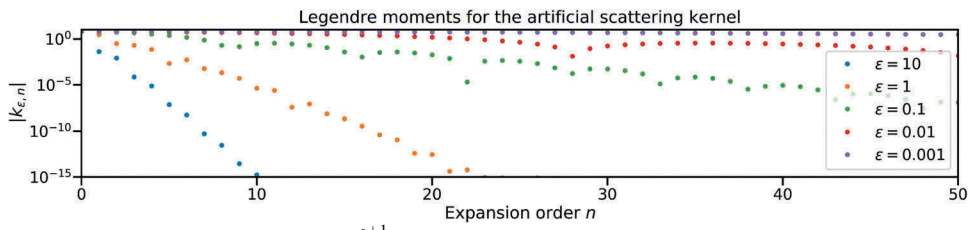


Fig. 3. Decay of the Legendre moments $k_{\varepsilon,n} = 2\pi \int_{-1}^{+1} s_{\varepsilon}(\mu) P_n(\mu) d\mu$ for different values of ε and the expansion order n.



III.E. Implementation Details

At this point, we choose a finite number of ordinates and moments; i.e., the flux ψ is now a vector with dimension N_q , and the moments ϕ have finite dimension N. Consequently, operators applied to the directional space become matrices. For better readability, we abuse notation and reuse the same symbols as before.

We observed that a second-order spatial scheme is required to capture the behavior of the test cases used in this work. To ensure an efficient sweeping step, we use a second-order upwind stencil without a limiter. Let us denote the operator L discretized in space and direction by L_{Δ} . For ease of presentation, we assume a slab geometry; i.e., we have the spatial variable $x \in \mathbb{R}$ and the directional variable $\mu \in [-1,1]$. In the following, we split the directional variable into $\mu_- \in [-1,0]$ and $\mu_+ \in (0,1]$. An extension to arbitrary dimension is straightforward. Now, with $\lambda_{\pm} = \mu_{\pm} \frac{\Delta t}{\Delta x}$ and $\sigma_t = \sigma_a + \sigma_s + \sigma_{as} + \frac{1}{\Delta t}$, we can write the discretized streaming operator as

$$L_{\Delta} \Psi = \lambda_{\pm} (g_{j+1/2} - g_{j-1/2}) + \Delta t \sigma_t \Psi.$$
 (26)

The numerical flux for μ_+ is then given by

$$g_{j+1/2} = a\psi_j + b\psi_{j-1}$$
, with $a = \frac{3}{2}, b = -\frac{1}{2}$ (27)

and for μ_{-} by

$$g_{j+1/2} = a\psi_{j+1} + b\psi_{j+2}. (28)$$

This scheme is L^2 stable, which we show in Appendix B. Let us now discuss the implementation of the implicit method in more detail. As mentioned earlier, a source iteration Eq. (25) is required to invert the operator $(L - \sigma_{as}S_{as}^+)$. For an initial guess $\psi^{(0)}$ and an arbitrary RHS R, this iteration is given by Algorithm 1.

Algorithm 1: Source Iteration Algorithm

1: **procedure** Source Iteration
$$[\psi^{(0)}, R]$$

2: $\ell \leftarrow 0$
3: $\psi^{(\ell+1)} \leftarrow L_{\Delta}^{-1} (\sigma_{as} S_{as}^+ \psi^{(\ell)} + R)$
4: **while** $\| \psi^{(\ell+1)} - \psi^{(\ell)} \|_2 \ge \epsilon \widetilde{c}$ **do**
5: $\psi^{(\ell+1)} \leftarrow L_{\Delta}^{-1} (\sigma_{as} S_{as}^+ \psi^{(\ell)} + R)$
6: $\ell \leftarrow \ell + 1$
return $\psi^{(\ell)}$

Note that the discrete artificial in-scattering S_{as}^+ is a sparse matrix, which guarantees an efficient evaluation of the matrix vector product $S_{as}^+ \psi^{(l)}$ in Eq. (25). Furthermore, the inverse of L_{Δ} can be computed by a sweeping procedure.

In order to get a good error estimator, in Algorithm 1, we set the constant $\tilde{c} = (1-T)/T$, where T is an estimate of the Lipschitz constant, and ϵ is a user-determined parameter. Using a generalized minimal residual method (GMRES) solver, our implementation solves the linear system of equations:

$$A\phi = b \tag{29a}$$

with

$$A = I - \sigma_s M (L - \sigma_{as} S_{as}^+)^{-1} O \Sigma$$
 (29b)

and

$$b = M(L - \sigma_{as}S_{as}^{+})^{-1}\widetilde{q}. \tag{29c}$$

The solver requires the evaluation of the LHS for a given ψ with an initial guess $\psi^{(0)}$, which is given by Algorithm 2.

Algorithm 2: Left-hand side of Eq. (29a)

```
    procedure LHS (ψ<sup>(0)</sup>, φ)
    \widetilde{\psi} ← SourceIteration[ψ<sup>(0)</sup>, σ<sub>s</sub> OΣφ]
    return φ − M\widetilde{\psi}
```

The main time-stepping scheme is then given by Algorithm 3.

Algorithm 3: Sweeping-Krylov algorithm

```
1: \psi^{\text{old}} \leftarrow \text{InitialCondition}()

2: \phi^{\text{old}} \leftarrow M\psi^{\text{old}}

3: while t < t_{\text{end}} do

4: b \leftarrow M \cdot \text{SourceIteration}(\psi^{\text{old}}, q + \frac{1}{\Delta t}\psi^{\text{old}})

5: \phi^{\text{new}} \leftarrow \text{Krylov}[\text{LHS}(\psi^{\text{old}}, \phi^{\text{old}}), b]

6: \psi^{\text{new}} \leftarrow \text{SourceIteration}(\psi^{\text{old}}, \sigma_s O \Sigma \phi^{\text{new}} + \frac{1}{\Delta t}\psi^{\text{old}})

7: \psi^{\text{old}} \leftarrow \psi^{\text{new}}

8: \phi^{\text{old}} \leftarrow \phi^{\text{new}}
```

After initializing ψ and ϕ , the RHS to Eq. (29a) is set up in line 4. Line 5 then solves the linear system Eq. (29a), and Line 6 determines the time-updated flux ψ from the moments ϕ^{new} .

There exist several ways to modify the presented algorithm to achieve higher performance. For example, one can modify the presented method by not fully converging the source iteration in Algorithm 1. Instead, only a single iteration can be performed to drive the moments φ and the respective angular flux ψ to their corresponding fixed points simultaneously. In numerical tests, we observe that this will significantly speed up the calculation. However, since we do not focus on run-time optimization, we do not further discuss this idea and leave it to future work.

IV. RESULTS

In the following, we evaluate the proposed method within the scope of two numerical test cases:

- 1. The line-source problem is used as it is inherently prone to ray effects when using the S_N method.
- 2. The lattice test case models (in a very simplified way) neutrons in a fission reactor with a source and heterogeneous materials.

For both problems, we present results for the explicit and implicit methods, respectively.

Both test cases are computed on a two-dimensional regular grid for the spatial variable. We project $\Omega_q \in \mathbb{S}^2$ for $q=1,\ldots,N_q$ onto the x-y plane.

The code used to compute the numerical results is published under the Massachusetts Institute of Technology license in a public repository at https://github.com/camminady/SN.

IV.A. Line-Source Test Case

The goal of this test case is to numerically compute the Green's function for an initial isotropic Dirac mass at the origin, i.e., $\psi(t=0,x,\Omega)=1/4\pi\delta(x)$, which is realized as a narrow Gaussian in space with $\psi(t=0,x,\Omega)=\max\{10^{-4},1/4\pi\delta\exp(-x^2/4\delta)\}$ and $\delta=0.03^2$. We choose $\sigma_s=\sigma_t=1$. The spatial discretization varies from 50×50 for a coarse grid to 200×200 points on the domain $[-1.5,1.5]\times[-1.5,1.5]$ for a fine grid. There exists a semianalytical solution to the full transport equation for this problem due to Ganapol et al. The exact solution consists of a circular front moving away from the origin as well as a tail of particles that have been scattered or not emitted perpendicularly from the center. We chose

the line source because it is a test case that lays bare almost any artifact from which an angular discretization might suffer.

The parameters of the artificial scattering have been set to $\varepsilon = \beta/N_q$ with N_q as the number of quadrature points. Obviously, choosing these parameters requires some experience. However, as in the case of filtering for P_N (Refs. 14 and 35), both parameters can be adjusted for coarse angular and spatial grids and are expected to be valid for finer grids, which seems to be the case for the line-source problem as well. The Courant-Friedrichs-Lewy (CFL) number, i.e., the ratio of the time step and the spatial cell size, is 0.95 for the explicit calculations and 2 for the implicit calculation. For the implicit discretization, the tolerance for the GMRES solver was set to 1.5×10^{-8} , and we considered the inner source iteration to be converged at an estimated error of 10^{-4} .

An overview of the analytics that we performed is

given in Fig. 4. We evaluate the scalar flux $\Phi(t, \mathbf{x}) = \int_{\mathbb{S}^2} \psi(t, \mathbf{x}, \mathbf{\Omega}') d\mathbf{\Omega}'$ at the final time step. We have performed an explicit S₄ computation with $N_q = 92$ and $N_x \times N_y = 200 \times 200$. In both rows of Fig. 4, the left column shows the scalar flux at the final time step. The first row shows the solution along cuts through the domain on the right with the respective cuts on the left in white. The second row shows the solution along circles with different radii on the right and the respective circles on the left. Strong oscillations are visible due to ray effects. For the first row, the analytical solution is given in green in the right column image. In the lower row, the analytical solution is constant along a circle with a certain radius,

In Figs. 5 and 6, we see the same summary of results, now for an explicit computation and an implicit computation, respectively. In both computations, ray effects have been reduced significantly when comparing the results with Fig. 4 despite the same number of quadrature points. The implicit calculation looks slightly more diffusive. However, the line-source problem is not a problem that would be computed implicitly in the first place, and we use it only to illustrate the expected behavior for implicit computations.

visualized for r = 0.2, r = 0.6, and r = 0.9 in green.

The values for β and ϵ in the fine calculations are determined from a parameter study using coarse spatial and angular grids. The results of this parameter study are given in Fig. 7 for the explicit algorithm and in Fig. 8 for the implicit algorithm.

A single simulation for the coarse configuration takes $\sim 1/400$ times the time of a single computation for the fine configuration. Consequently, the full parameter study with

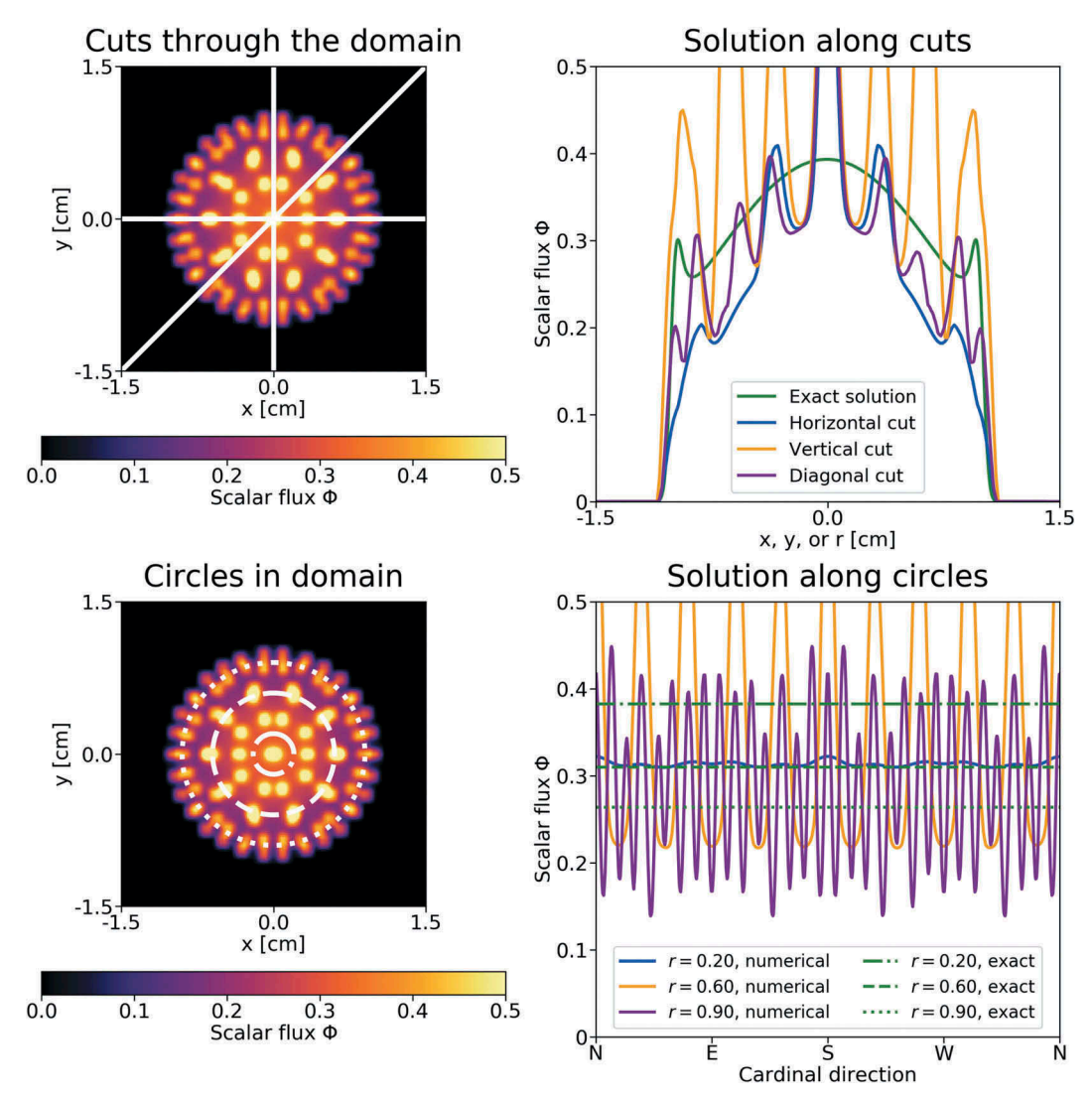


Fig. 4. The S_4 solution (using an explicit time discretization) with ray effects. We choose $N_q = 92$ quadrature points, the spatial domain is composed of $N_x \times N_y = 200 \times 200$ spatial cells, and the CFL number is 0.95. Cuts through the domain and along circles with different radii are visualized in the right column. Only the solution along the horizontal cut is symmetric for the icosahedron quadrature.

all 306 configurations can be performed for less than the costs of a single fine computation. For the optimal parameter configuration, the error decreases down to 37.8% for the explicit case and down to 41.4% for the implicit case.

In both cases, implicit and explicit, we observe a region of parameters that yield similarly good results. This behavior mostly matches the predicted relation from the asymptotic analysis; i.e., when ε is small, $\sigma_{as} \cdot \varepsilon$ controls the effect of artificial scattering.

We also investigate the performance of the as- S_N method when measured in run time and in memory consumption. Consider therefore the results presented in Figs. 9 and 10, which summarize the results for the line-source test case computed with the S_N and as- S_N methods for different values of N. Figure 9 measures the error between the numerical

solution and the analytical solution in the L^2 norm, called δ_1 . Figure 10 considers the H^1 seminorm. We observe an increase in run time when activating artificial scattering but a decrease in the errors δ_1 and δ_2 . On the right, the errors are plotted against the number of ordinates, which ultimately dictates the memory consumption. For example, an S_8 computation takes about as long as an as- S_5 computation and yields a similar δ_1 error. However, the number of ordinates can be reduced from 492 to 162. For both δ_1 and δ_2 , the effect of artificial scattering vanishes in the limit of $N_q \to \infty$.

IV.B. Lattice Test Case

We also investigate the lattice test case, ^{9,36} depicted in Fig. 11. A constant, isotropic source is placed in the center



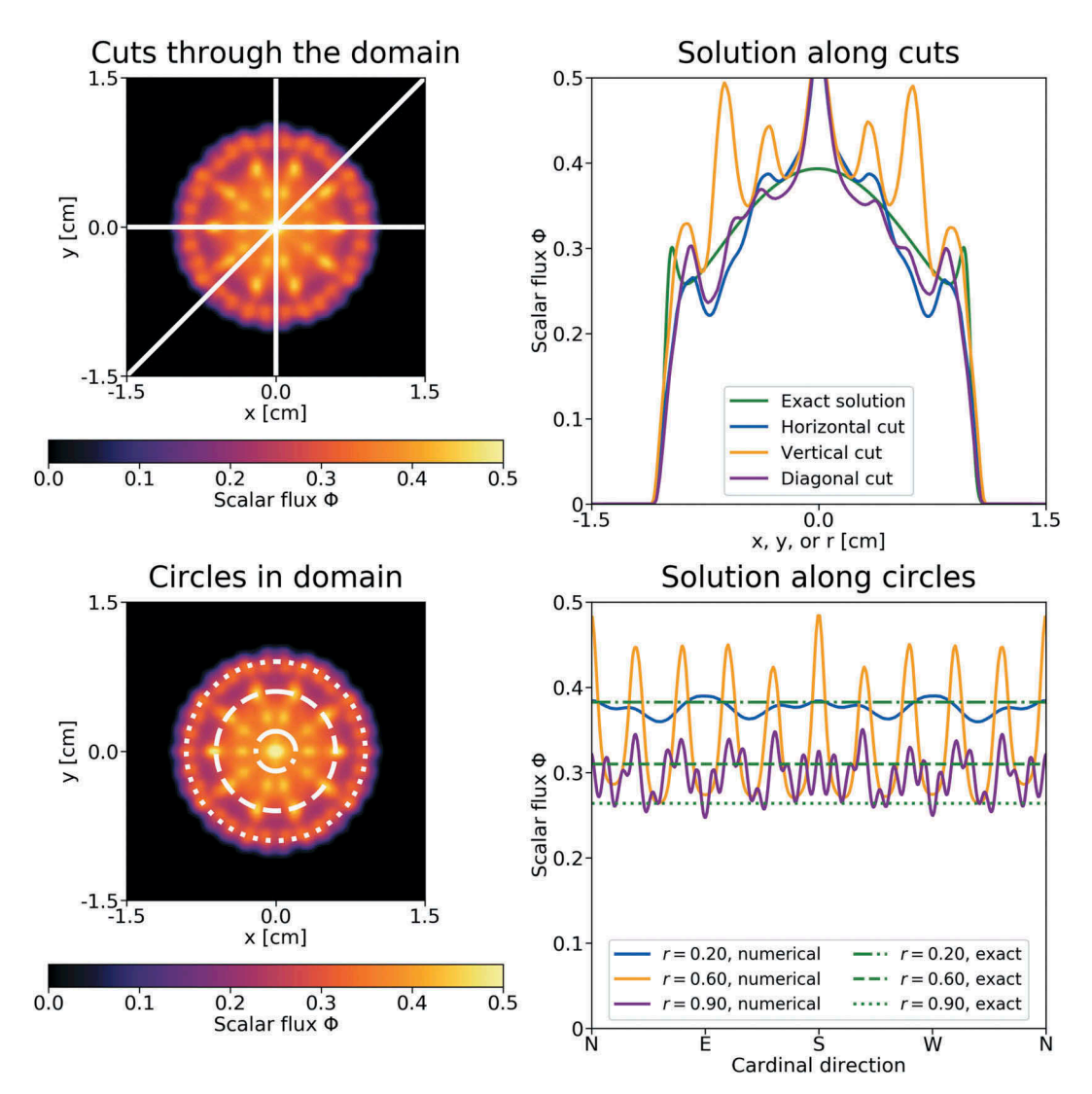


Fig. 5. The as- S_4 solution (using an explicit time discretization) with mitigated ray effects. We choose $N_q = 92$ quadrature points, the spatial domain is composed of $N_x \times N_y = 200 \times 200$ spatial cells, and the CFL number is 0.95. Cuts through the domain and along circles with different radii are visualized in the right column. We set $\sigma_{as} = 5$ and $\beta = 4.5$. Only the solution along the horizontal cut is symmetric for the icosahedron quadrature.

of the domain in the orange square. In the white cells, the material is purely scattering whereas the orange and black squares are purely absorbing. The boundary conditions are vacuum. All test case parameters are listed in Table I.

In Fig. 12, we see the as- S_4 solution to the lattice problem on the left, the S_{15} solution in the center, and the S_4 solution on the right. Here, S_{15} uses 1962 ordinates while S_4 and as- S_4 use 92 ordinates.

We take the S_{15} solution with $N_q=1962$ as our reference solution. When comparing the as- S_4 solution with the S_4 solution, we see an improvement in the solution quality. Ray effects are better mitigated in regions where the scalar flux is small. The number of ordinates is kept constant.

TABLE I

Material Properties for the Lattice Test Case*

Color	$\sigma_a(\mathrm{cm}^{-1})$	$\sigma_s(\mathrm{cm}^{-1})$	$Q(\text{cm}^{-2}\cdot\text{s}^{-1})$
White	0	1	0
Black	10	0	0
Orange	10	0	1

^{*}The domain is of size $[0 \text{ cm}, 7 \text{ cm}]^2$, and $t_{end} = 3.2 \text{ s}$.

Additionally, Fig. 13 puts the as- S_4 solution and the S_{15} solution side by side in the center frame. Minor ray effects are visible when looking at the white isoline. However, the number of ordinates has been reduced by a factor of ~ 21 .



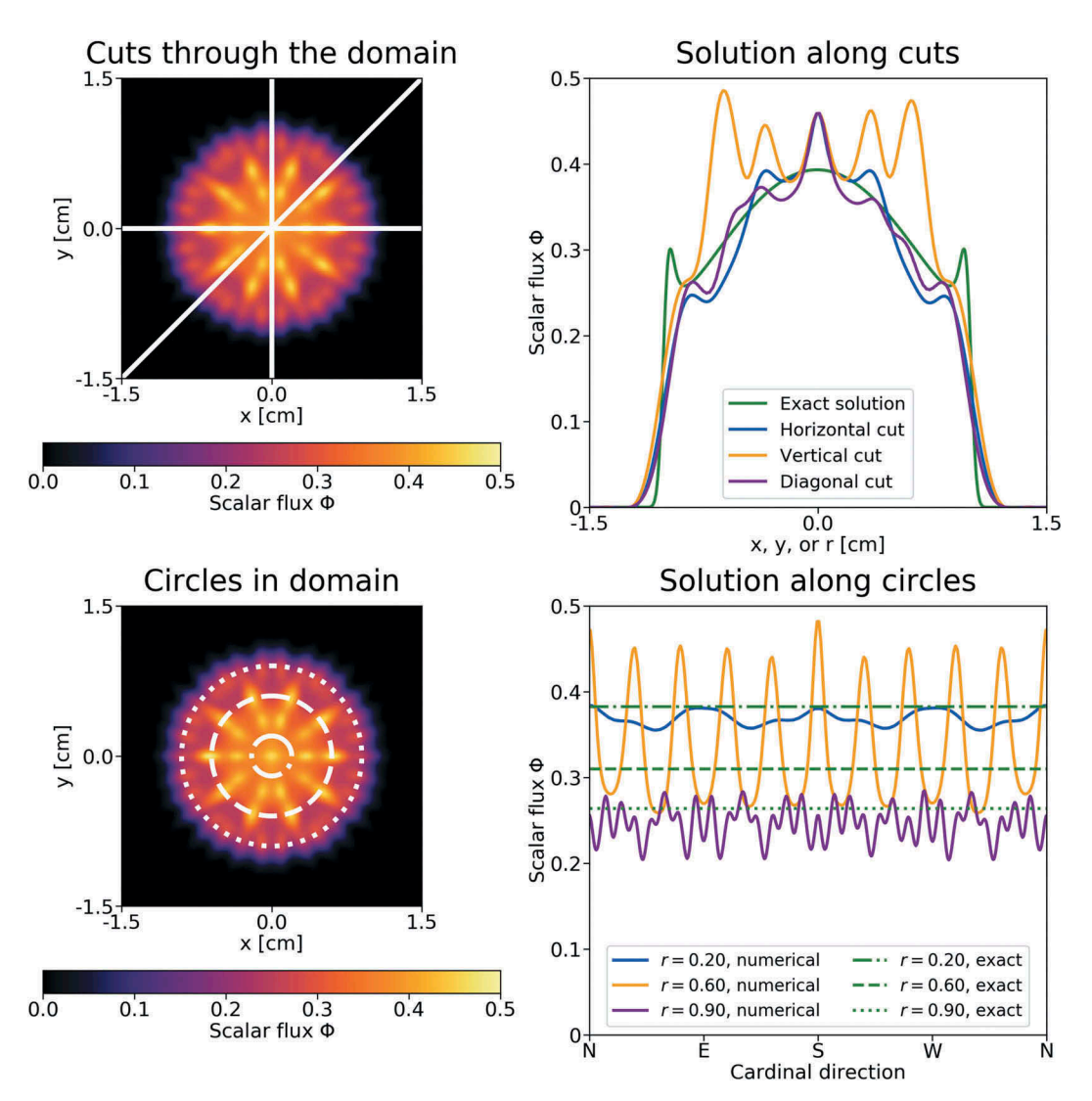


Fig. 6. The as- S_4 solution (using an implicit time discretization) with mitigated ray effects. We choose $N_q = 92$ quadrature points, the spatial domain is composed of $N_x \times N_y = 200 \times 200$ spatial cells, and the CFL number is 2. Cuts through the domain and along circles with different radii are visualized in the right column. We set $\sigma_{as} = 7$ and $\beta = 4$. Only the solution along the horizontal cut is symmetric for the icosahedron quadrature.

Similar to the line-source test case, we set $\beta = 4.5$ and $\sigma_{as} = 5.0$ for explicit calculation, and we set $\beta = 4.0$ and $\sigma_{as} = 7.0$ for the implicit calculation.

We also perform simulations for the lattice problem with the implicit time discretization. However, since the chosen scheme is only L² stable, the solution becomes negative for the lattice test case as illustrated in Fig. 14. Nevertheless, Fig. 15 demonstrates the inherent advantage when performing implicit computations: We are able to use a very large CFL number, thus reducing the number of time steps and the overall computational costs drastically. Note that the scheme preserves positivity for the chosen CFL numbers.

V. CONCLUSION AND OUTLOOK

We have presented a new ray effect mitigation technique that relies on an additional, artificial scattering operator introduced into the radiative transfer equation. When the number of ordinates tends to infinity, the artificial scattering vanishes, and the modified equation reduces to the original transport equation. In this case, when choosing the product of the scattering strength and the variance constant, the term tending to zero with the slowest rate is the Fokker-Planck operator.

The artificial scattering operator can be integrated into standard S_N codes. Solution algorithms, both for



Baseline normalized L^2 error of Φ over the full domain.

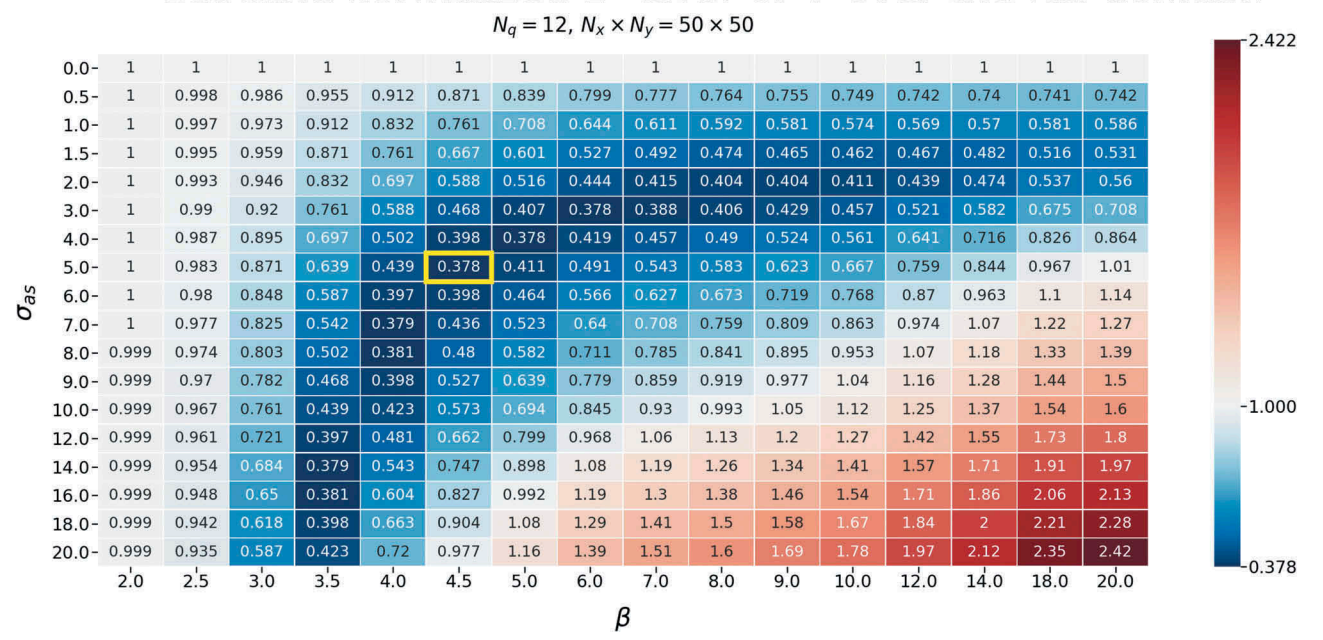


Fig. 7. Parameter study for σ_{as} and $\varepsilon = \beta/N_q$ on a grid of $N_q \times N_x \times N_y = 12 \times 50 \times 50$ in an explicit calculation. For every simulation we compute the L² error of the scalar flux Φ with respect to a semianalytical reference solution on the same spatial grid. The number in each field of the heat map is then the baseline normalized error, i.e., the L² error obtained for that specific parameter configuration divided by the error obtained without artificial scattering. For the case of $\beta = 4.5$ and $\sigma_{as} = 5$ (highlighted in yellow), the error drops down to 37.8% of the original error without artificial scattering.

Baseline normalized L^2 error of Φ over the full domain.

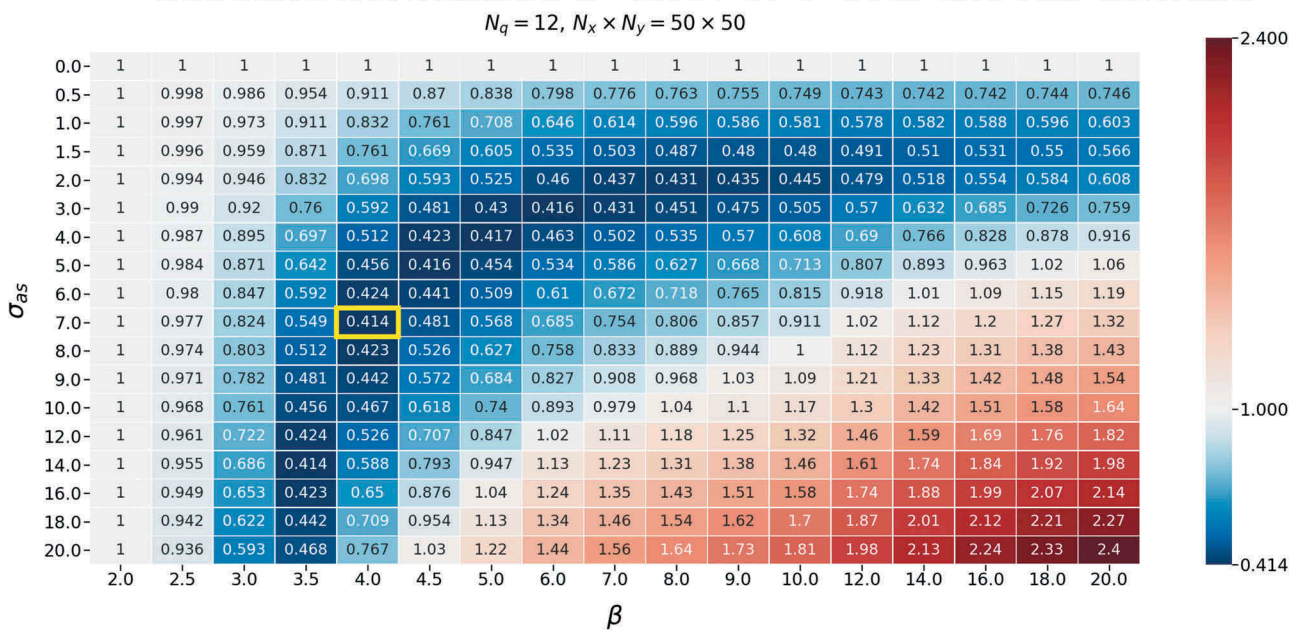


Fig. 8. Parameter study for σ_{as} and $\varepsilon = \beta/N_q$ on a grid of $N_q \times N_x \times N_y = 12 \times 50 \times 50$ in an implicit calculation. For every simulation we compute the L² error of the scalar flux Φ with respect to a semianalytical reference solution on the same spatial grid. The number in each field of the heat map is then the baseline normalized error, i.e., the L² error obtained for that specific parameter configuration divided by the error obtained without artificial scattering. For the case of $\beta = 4$ and $\sigma_{as} = 7$ (highlighted in yellow), the error drops down to 41.4% of the original error without artificial scattering.



Error δ_1 for the line-source test case

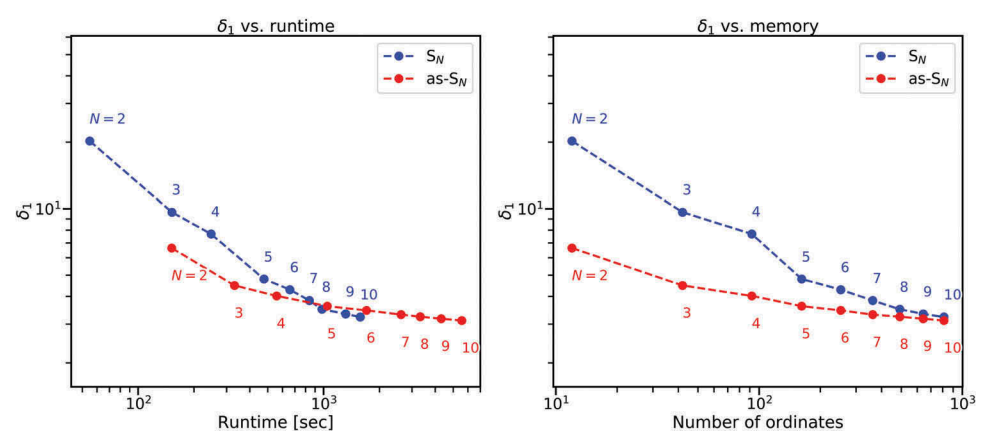


Fig. 9. We computed $\delta_1 = \|\Phi_{numerical} - \Phi_{analytical}\|_2$ for the line-source test case using the implicit S_N and as- S_N method for $N_x \times N_y = 200 \times 200$. Computations were performed on a quad core Intel[®] i5-7300U CPU (2.60 GHz) with 12-GB memory.

Error δ_2 for the line-source test case

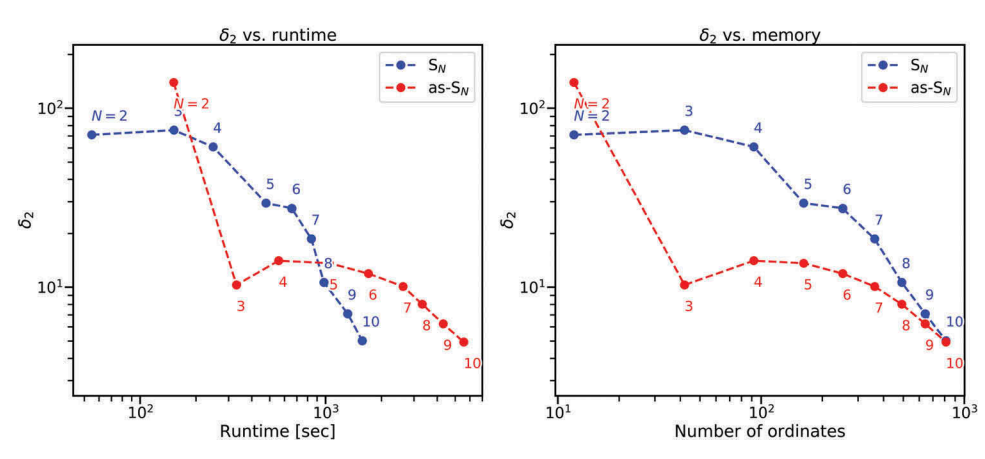


Fig. 10. We computed $\delta_2 = \|\nabla \Phi_{numerical} - \nabla \Phi_{analytical}\|_2$ for the line-source test case using the implicit S_N and as- S_N method for $N_x \times N_y = 200 \times 200$. Computations were performed on a quad core Intel[®] i5-7300U CPU (2.60 GHz) with 12-GB memory.

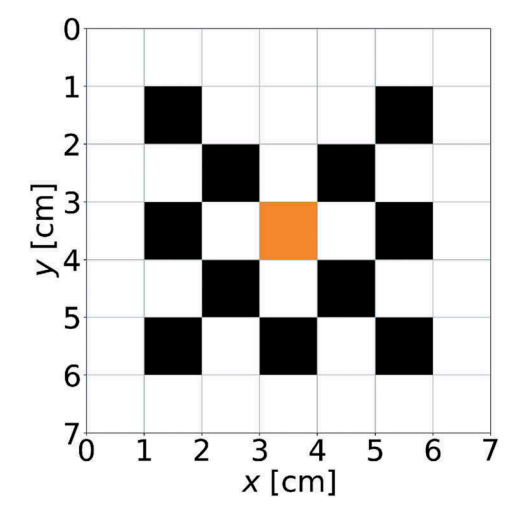


Fig. 11. Layout of the lattice test case. Different materials (black, white, orange) with the source in the center (orange).

the explicit case and the implicit case, have been presented and rigorously analyzed in the nonstandard, implicit case. To avoid using a large number of moments for the Krylov solver in the implicit case, we propose to invert the artificial scattering operator by a source iteration.

We have presented numerical results for the line-source and lattice test case. The results demonstrate that artificial scattering yields the same accuracy as S_N but for a reduced number of ordinates.

For the second-order implicit computations, the solutions might turn negative since L^2 stability does not guarantee positivity of the solution. However, when choosing a sufficiently large CFL number, the solution values in our numerical experiments remain positive. A rigorous investigation of this effect and possibly the derivation of a CFL number ensuring positivity is left to future work.



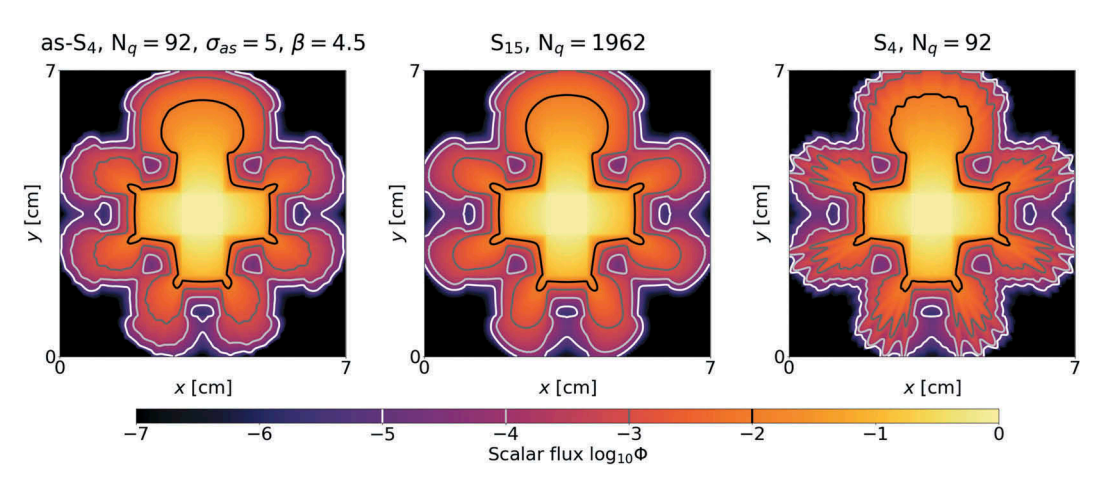


Fig. 12. Comparison for the lattice test case at $t_{end} = 3.2$ s. Left: the as-S₄ solution for the optimal parameter choice; center: the S₁₅ solution; right: the S₄ solution. Isolines are drawn at four different levels, highlighted inside the color bar. We used 280×280 spatial cells.

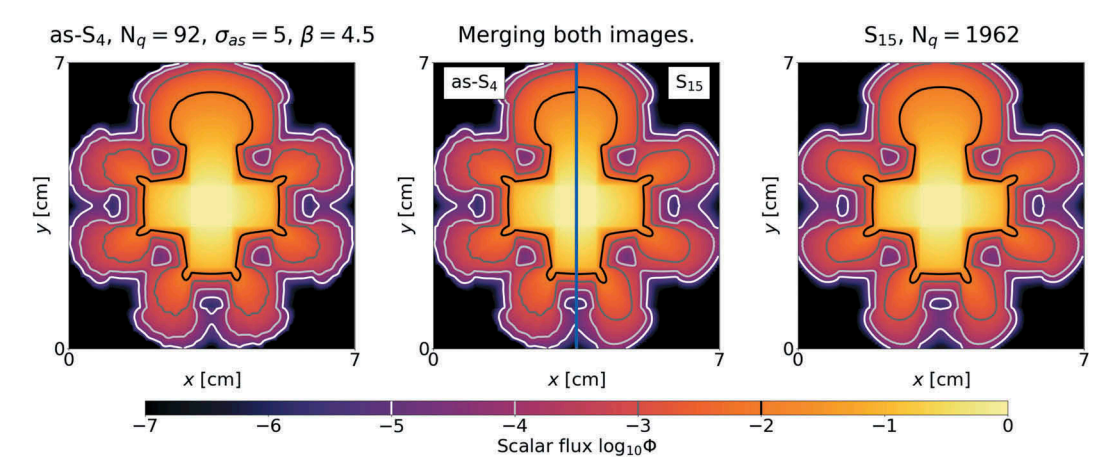


Fig. 13. Comparison for the lattice test case at $t_{end} = 3.2$ s. Left: the as-S₄ solution; right: the S₁₅ solution; center: the image merges the left half of the left image with the right half of the right image. Isolines are drawn at four different levels, highlighted inside the color bar. We used 280×280 spatial cells.

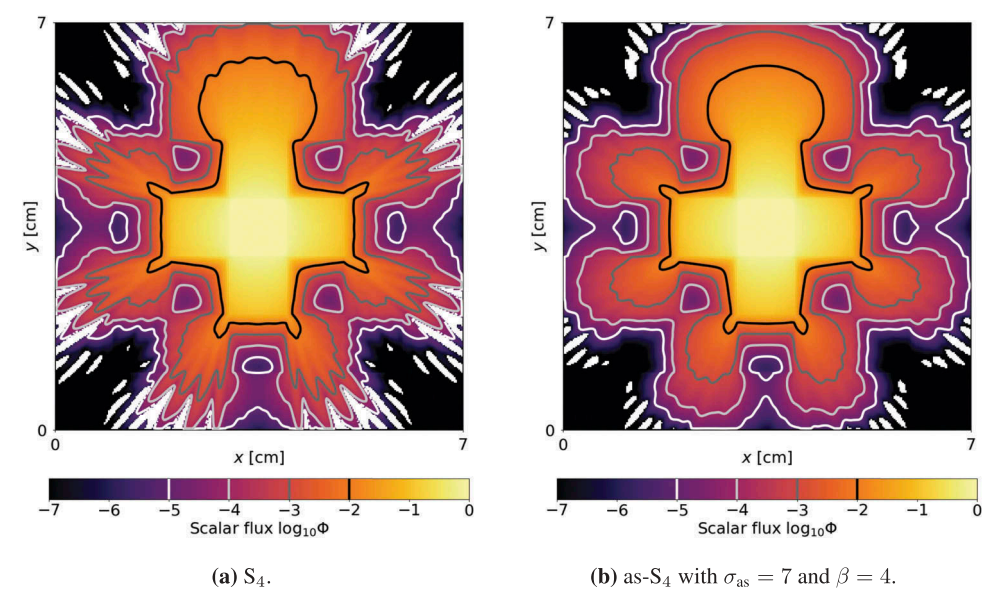


Fig. 14. Solutions to the lattice problem with an implicit computation for a CFL number of 2, $N_q = 92$, and $N_x \times N_y = 280 \times 280$. The white regions indicate negativity of the solution.



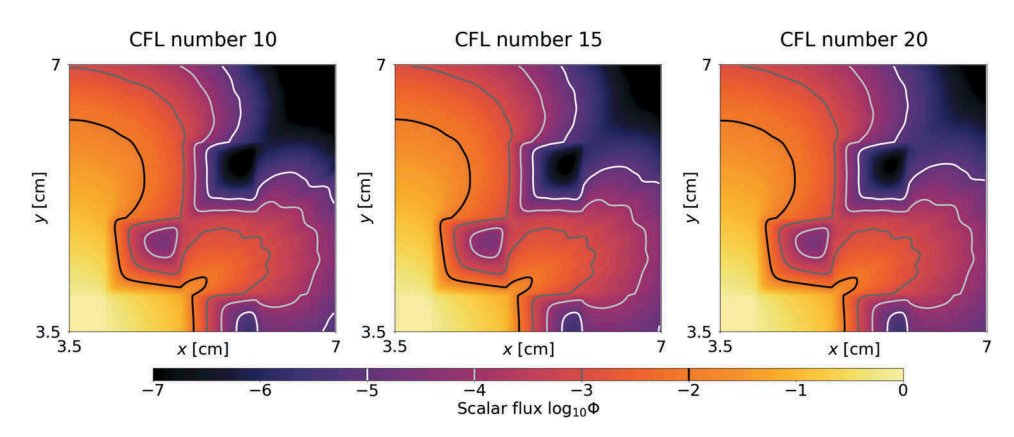


Fig. 15. Solutions to the lattice problem with an implicit computation for different CFL numbers and $N_q = 92$, $N_x \times N_y = 280 \times 280$, $\sigma_{as} = 7$, and $\beta = 4$. Zoom into the region $[3.5, 7] \times [3.5, 7]$.

Note that our test cases chose a constant value for the artificial scattering strength; however, it seems plausible to make this strength spatially dependent to ensure that artificial scattering is turned on only when required. It remains to demonstrate the feasibility of the as- S_N method in real-world applications using large-scale, highly parallelizable codes.

APPENDIX A ICOSAHEDRON QUADRATURE

The quadrature points and weights for the quadrature in Sec. III.C are given for order 2 (12 quadrature points). Every line contains four entries: the x, y, and z positions, and the quadrature weight (see Table A.I.). The quadrature weights sum to 4π . All entries are in double precision. The quadratures for order 2, order 3 (42 quadrature points), order 4 (92 quadrature points),

and order 5 (162 quadrature points) can be downloaded as .txt files from a public repository at github.com/camminady/IcosahedronQuadrature.

APPENDIX B IMPLICIT SECOND-ORDER UPWIND SCHEME

In the following, we show that the chosen numerical flux is L^2 stable. For simplicity, we look at the one-dimensional advection equation:

$$\partial_t \Psi + \Omega \partial_x \Psi = 0 \tag{B.1}$$

with $\Omega \in \mathbb{R}_+$. A finite volume discretization is given by

$$\psi_i^{n+1} = \psi_i^n - \lambda (g_{i+1/2} - g_{i-1/2}), \qquad (B.2)$$

TABLE A.I
Sample of the Icosahedron Quadrature Set

x	у	z	w
+0.00000000000000000000000000000000000	+0.00000000000000000000000000000000000	+1.000000000000000000000000000000000000	+0.7370796188178727 +0.7370796188178727 +1.3293827143261787 +1.3293827143261787 +1.0751303204457423 +1.0751303204457423
+0.00000000000000000000000000000000000	+0.8944271909999159 +0.4472135954999580 +0.4472135954999580 +0.0000000000000000000000000000000000	$\begin{array}{c} -0.4472135954999580 \\ -0.7236067977499790 \\ -0.7236067977499790 \\ -1.00000000000000000 \\ -0.4472135954999580 \\ -0.4472135954999580 \end{array}$	+0.7370796188178727 +1.3293827143261787 +1.3293827143261787 +0.7370796188178727 +1.0751303204457423 +1.0751303204457423



where we use $\lambda = \Omega \Delta t / \Delta x$. A second-order, implicit numerical flux is given by

$$g_{j+1/2} = a\psi_j^{n+1} + b\psi_{j-1}^{n+1}$$
 (B.3)

with

$$a = \frac{3}{2}$$
 and $b = -\frac{1}{2}$. (B.4)

Let us check if the scheme dissipates the L^2 entropy $\eta(\psi) = \psi^2/2$. For this, we multiply our scheme Eq. (B.2) with ψ_i^{n+1} ; i.e., we obtain

$$\psi_j^{n+1}\psi_j^{n+1} = \psi_j^n\psi_j^{n+1} - \lambda(g_{j+1/2} - g_{j-1/2})\psi_j^{n+1}.$$
 (B.5)

Now, one needs to remove the cross term $\psi_j^n \psi_j^{n+1}$, which can be done by reversing the binomial formula:

$$\psi_j^n \psi_j^{n+1} = \frac{1}{2} (\psi_j^{n+1})^2 + \frac{1}{2} (\psi_j^n)^2 - \frac{1}{2} (\psi_j^{n+1} - \psi_j^n)^2.$$
 (B.6)

Plugging this formulation for the cross term into Eq. (B.5) and making use of the definition of the square entropy η gives

$$\eta(\psi_j^{n+1}) = \eta(\psi_j^n) - \frac{1}{2} (\psi_j^{n+1} - \psi_j^n)^2
- \lambda (g_{j+1/2} - g_{j-1/2}) \psi_j^{n+1} .$$
(B.7)

This shows that in order to achieve entropy dissipation, i.e.,

$$\sum_{i=1}^{N_x} \eta(\psi_j^{n+1}) \le \sum_{i=1}^{N_x} \eta(\psi_j^{n+1}), \tag{B.8}$$

we need

$$\mathcal{E} = \sum_{j=1}^{N_{\mathrm{x}}} \frac{1}{2} (\psi_j^{n+1} - \psi_j^n)^2 + \lambda \sum_{j=1}^{N_{\mathrm{x}}} (g_{j+1/2} - g_{j-1/2}) \psi_j^{n+1} \overset{!}{\geq} 0 \,.$$

Note that the first term of \mathcal{E} , which essentially comes from the implicit time discretization, is always positive. It remains to be shown that $\sum_{j=1}^{N_x} (g_{j+1/2} - g_{j-1/2}) \psi_j^{n+1}$ is positive as well. Let us rewrite this term for all spatial cells as a matrix vector product. That is, when collecting the solution at time step n+1 for all N_x spatial cells in a vector $\psi \in \mathbb{R}^{N_x}$, this term becomes

$$\sum_{j=1}^{N_x} \left(\left(g_{j+1/2} - g_{j-1/2} \right) \psi_j^{n+1} \right) = \psi^T B \psi , \qquad (B.9)$$

where $B \in \mathbb{R}^{N_x \times N_x}$ is a lower triangular matrix. This product can be symmetrized with $S = \frac{1}{2}(B + B^T)$, meaning that we have $\psi^T B \psi = \psi^T S \psi$. For our stencil, the matrix S has entries $s_{jj} = \frac{3}{2}$ on the diagonal and $s_{j,j-1} = s_{j-1,j} = -1$ as $s_{j,j-2} = s_{j-2,j} = \frac{1}{4}$ on the lower and upper diagonals. Positivity of $\psi^T S \psi$ and thereby of the entropy dissipation term \mathcal{E} is guaranteed if S is positive definite, i.e., has positive eigenvalues. The eigenvalues for S have been computed numerically to verify positivity in Fig. B.1.

Acknowledgments

The authors wish to thank Ryan G. McClarren (University of Notre Dame) for many fruitful discussions.

This material is based upon work supported by the National Science Foundation under Grant No. 1913277 and by UT-Battelle, LLC, under Contract No. DE-AC0500OR22725 with the U.S. Department of Energy. The United States Government retains and the publisher, by accepting the article for publication, acknowledges that the United States Government retains a non-exclusive, paid-up, irrevocable, world-wide license to publish or reproduce the published form of this manuscript, or allow others to do so, for the United States Government purposes. The

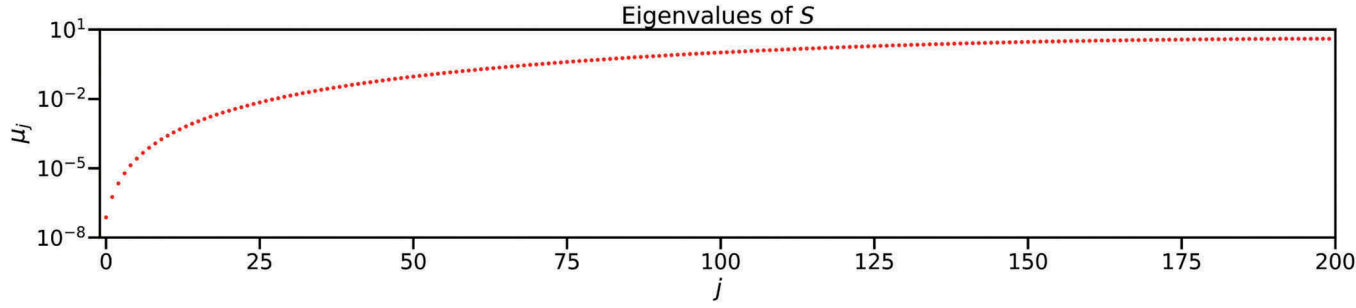


Fig. B.1. Eigenvalues of S for $N_x = 200$. All eigenvalues remain positive.



Department of Energy will provide public access to these results of federally sponsored research in accordance with the DOE Public Access Plan (http://energy.gov/downloads/doe-public-access-plan).

References

- 1. J. J. DUDERSTADT, Nuclear Reactor Analysis, Wiley (1976).
- A. F. HENRY, C. SCOTT, and S. MOORTHY, "Nuclear Reactor Analysis," *IEEE Trans. Nucl. Sci.*, 24, 6, 2566 (1977); https://doi.org/10.1109/TNS.1977.4329257.
- 3. R. LOWRIE, J. MOREL, and J. HITTINGER, "The Coupling of Radiation and Hydrodynamics," *Astrophys. J.*, **521**, *1*, 432 (1999); https://doi.org/10.1086/apj.1999.521.issue-1.
- R. G. McCLARREN and R. B. LOWRIE, "Manufactured Solutions for the P1 Radiationhydrodynamics Equations,"
 J. Quant. Spectrosc. Radiat. Transfer, 109, 15, 2590 (2008); https://doi.org/10.1016/j.jqsrt.2008.06.003.
- 5. C. L. FRYER, G. ROCKEFELLER, and M. S. WARREN, "SNSPH: A Parallel Three-Dimensional Smoothed Particle Radiation Hydrodynamics Code," *Astrophys. J.*, **643**, *1*, 292 (2006); https://doi.org/10.1086/apj.2006.643.issue-1.
- F. D. SWESTY and E. S. MYRA, "A Numerical Algorithm for Modeling Multigroup Neutrino-Radiation Hydrodynamics in Two Spatial Dimensions," *Astrophys. J. Suppl. Ser.*, 181, 1, 1 (2009); https://doi.org/10.1088/0067-0049/181/1/1.
- 7. M. K. MATZEN et al., "Pulsed-Power-Driven High Energy Density Physics and Inertial Confinement Fusion Research," *Phys. Plasmas*, **12**, *5*, 055503 (2005); https://doi.org/10.1063/1.1891746.
- 8. M. MARINAK et al., "Three-Dimensional HYDRA Simulations of National Ignition Facility Targets," *Phys. Plasmas*, **8**, 5, 2275 (2001); https://doi.org/10.1063/1. 1356740.
- 9. T. A. BRUNNER, "Forms of Approximate Radiation Transport," SAND2002-1778, Sandia National Laboratories (2002).
- 10. K. M. CASE and P. F. ZWEIFEL, *Linear Transport Theory*, Addison-Wesley Series in Nuclear Science and Engineering. Addison-Wesley, Reading, Massachusetts (1967).
- 11. G. C. POMRANING, *The Equations of Radiation Hydrodynamics*, Courier Corporation (1973).
- 12. E. E. LEWIS and W. F. MILLER, Computational Methods of Neutron Transport, Wiley (1984).
- R. G. McCLARREN, J. P. HOLLOWAY, and T. A. BRUNNER, "On Solutions to the P_n Equations for Thermal Radiative Transfer," J. Comput. Phys., 227, 5, 2864 (2008); https://doi.org/10.1016/j.jcp.2007.11.027.
- 14. R. G. McCLARREN and C. D. HAUCK, "Robust and Accurate Filtered Spherical Harmonics Expansions for

- Radiative Transfer," *J. Comput. Phys.*, **229**, *16*, 5597 (2010); https://doi.org/10.1016/j.jcp.2010.03.043.
- 15. K. D. LATHROP, "Ray Effects in Discrete Ordinates Equations," *Nucl. Sci. Eng.*, **32**, *3*, 357 (1968); https://doi.org/10.13182/NSE68-4.
- 16. J. MOREL et al., "Analysis of Ray-Effect Mitigation Techniques," *Nucl. Sci. Eng.*, **144**, *I*, 1 (2003); https://doi.org/10.13182/NSE01-48.
- 17. K. A. MATHEWS, "On the Propagation of Rays in Discrete Ordinates," *Nucl. Sci. Eng.*, **132**, *2*, 155 (1999); https://doi.org/10.13182/NSE99-A2057.
- 18. I. ABU-SHUMAYS, "Angular Quadratures for Improved Transport Computations," *Transp. Theory Stat. Phys.*, **30**, 2–3, 169 (2001); https://doi.org/10.1081/TT-100105367.
- 19. K. LATHROP, "Remedies for Ray Effects," *Nucl. Sci. Eng.*, **45**, *3*, 255 (1971); https://doi.org/10.13182/NSE45-03-255.
- 20. J. JUNG et al., "Discrete Ordinate Neutron Transport Equation Equivalent to *P_L* Approximation," *Nucl. Sci. Eng.*, **49**, *I*, 1 (1972); https://doi.org/10.13182/NSE49-01-01.
- 21. W. H. REED, "Spherical Harmonic Solutions of the Neutron Transport Equation from Discrete Ordinate Codes," *Nucl. Sci. Eng.*, **49**, *1*, 10 (1972); https://doi.org/10.13182/NSE72-A22523.
- 22. W. MILLER Jr. and W. H. REED, "Ray-Effect Mitigation Methods for Two-Dimensional Neutron Transport Theory," *Nucl. Sci. Eng.*, **62**, *3*, 391 (1977); https://doi.org/10.13182/NSE62-391.
- 23. J. TENCER, "Ray Effect Mitigation Through Reference Frame Rotation," *J. Heat Transfer*, **138**, *11*, 112701 (2016); https://doi.org/10.1115/1.4033699.
- 24. T. CAMMINADY et al., "Ray Effect Mitigation for the Discrete Ordinates Method Through Quadrature Rotation," *J. Comput. Phys.*, **382**, 105 (2019); https://doi.org/10.1016/j.jcp.2019.01.016.
- 25. R. J. LeVEQUE, *Numerical Methods for Conservation Laws*, Springer (1992).
- G. L. OLSON, "Second-Order Time Evolution of P_N Equations for Radiation Transport," J. Comput. Phys., 228, 8, 3072 (2009); https://doi.org/10.1016/j.jcp.2009.01.012.
- 27. C. HAUCK and V. HENINGBURG, "Filtered Discrete Ordinates Equations for Radiative Transport," *J. Sci. Comput.*, **80**, *1*, 614 (2019); https://doi.org/10.1007/s10915-019-00950-1.
- 28. M. FRANK, C. HAUCK, and K. KÜPPER, "Convergence of Filtered Spherical Harmonic Equations for Radiation Transport," *Commun. Math. Sci.*, **14**, *5*, 1443 (2016); https://doi.org/10.4310/CMS.2016.v14.n5.a10.
- 29. G. POMRANING, "The Fokker-Planck Operator as an Asymptotic Limit," *Math. Models Meth. Appl. Sci.*, **2**, *1*, 21 (1992); https://doi.org/10.1142/S021820259200003X.



- 30. C. K. GARRETT and C. D. HAUCK, "A Comparison of Moment Closures for Linear Kinetic Transport Equations: The Line Source Benchmark," *Transp. Theory Stat. Phys.*, **42**, 6–7, 203 (2013); https://doi.org/10.1080/00411450.2014. 910226.
- 31. T. CAMMINADY, M. FRANK, and J. KUSCH, "Highly Uniform Quadrature Sets for the Discrete Ordinates Method," *Proc. Int. Conf. Mathematics and Computational Methods Applied to Nuclear Science and Engineering*, Portland, Oregon, August 25–29, 2019, American Nuclear Society (2019).
- 32. V. FABER and T. A. MANTEUFFEL, "A Look at Transport Theory from the Point of View of Linear Algebra," Los Alamos National Laboratory (1988).
- 33. S. ASHBY et al., "Preconditioned Iterative Methods for Discretized Transport Equations," *Proc. Int. Topl. Mtg.*

- Advances in Mathematics, Computations, and Reactor Physics, Pittsburgh, Pennsylvania, April 28–May 2, 1991, Vol. 2, p. 2–1, American Nuclear Society (1991).
- 34. B. GANAPOL et al., "Homogeneous Infinite Media Time-Dependent Analytical Benchmarks," Los Alamos National Laboratory (2001).
- 35. V. M. LABOURE, R. G. McCLARREN, and C. D. HAUCK, "Implicit Filtered P_N for High-Energy Density Thermal Radiation Transport Using Discontinuous Galerkin Finite Elements," *J. Comput. Phys.*, **321**, 624 (2016); https://doi.org/10.1016/j.jcp.2016.05.046.
- 36. T. A. BRUNNER and J. P. HOLLOWAY, "Two-Dimensional Time Dependent Riemann Solvers for Neutron Transport," *J. Comput. Phys.*, **210**, *1*, 386 (2005); https://doi.org/10.1016/j.jcp.2005.04.011.

